



## Light scattering on the structural characterization of DMPG vesicles along the bilayer anomalous phase transition

Thais A. Enoki, Vera B. Henriques, M. Teresa Lamy\*

Instituto de Física, Universidade de São Paulo, CP 66318, CEP 05314-970, São Paulo, SP, Brazil

### ARTICLE INFO

#### Article history:

Received 25 September 2012

Received in revised form 2 November 2012

Accepted 6 November 2012

Available online 16 November 2012

#### Keywords:

DMPG

Static light scattering

Dynamic light scattering

Gel–fluid transition region

Perforated vesicle

Charged lipid bilayer

### ABSTRACT

Highly charged vesicles of the saturated anionic lipid dimyristoyl phosphatidylglycerol (DMPG) in low ionic strength medium exhibit a very peculiar thermo-structural behavior. Along a wide gel–fluid *transition region*, DMPG dispersions display several anomalous characteristics, like low turbidity, high electrical conductivity and viscosity. Here, static and dynamic light scattering (SLS and DLS) were used to characterize DMPG vesicles at different temperatures. Similar experiments were performed with the largely studied zwitterionic lipid dimyristoyl phosphatidylcholine (DMPC). SLS and DLS data yielded similar dimensions for DMPC vesicles at all studied temperatures. However, for DMPG, along the gel–fluid *transition region*, SLS indicated a threefold increase in the vesicle radius of gyration, whereas the hydrodynamic radius, as obtained from DLS, increased 30% only. Despite the anomalous increase in the radius of gyration, DMPG lipid vesicles maintain isotropy, since no light depolarization was detected. Hence, SLS data are interpreted regarding the presence of isotropic vesicles within the DMPG anomalous transition, but highly perforated vesicles, with large holes. DLS/SLS discrepancy along the DMPG *transition region* is discussed in terms of the interpretation of the Einstein–Stokes relation for porous vesicles. Therefore, SLS data are shown to be much more appropriate for measuring porous vesicle dimensions than the vesicle diffusion coefficient. The underlying nanoscopic process which leads to the opening of pores in charged DMPG bilayer is very intriguing and deserves further investigation. One could envisage biotechnological applications, with vesicles being produced to enlarge and perforate in a chosen temperature and/or pH value.

© 2012 Elsevier Ireland Ltd. All rights reserved.

### 1. Introduction

Thermal properties of lipid bilayers have been extensively studied, not only due to their biological relevance but also in relation to the interesting fundamental physicochemical problem of lipid–lipid interaction in aqueous media. Knowledge of the thermal behavior of a lipid membrane is central for the understanding of its structure. It is well-known that most saturated lipids present a cooperative thermal transition, called main transition, at a temperature which is dependent on hydrocarbon chain interactions, that is, on the number of C-atoms in the chains, and on head-group interactions. The latter depends on the size and charge of the headgroup, and their interactions at the water surface, such as hydrogen or ion-bonding (see, for instance, Marsh, 1990). In particular, multilamellar vesicles of the *zwitterionic* lipid dimyristoyl phosphatidylcholine (DMPC; two saturated chains of 14-C atoms each) present a highly cooperative gel–fluid transition at around 23 °C, detected as a very narrow peak by differential scanning

calorimetry (DSC). Besides the main transition, at lower temperatures, a small DSC peak is identified as the beginning of the bilayer melting process, and associated to a pre-transition to a ripple (mainly gel) phase (Janiak et al., 1979; Riske et al., 2009a, 2009b). Here we shall focus our interest on the main thermal transition, which we shall term a “gel–fluid” transition, which stresses the chain origin of this order–disorder transition.

Freshly prepared dispersions of the saturated anionic phospholipid dimyristoyl phosphatidylglycerol (DMPG) at high ionic strength (around 100 mM, with  $\text{PG}^-$  groups electrostatically shielded), and pH values higher than 5, display behavior very similar to that of zwitterionic DMPC, presenting a rather cooperative gel–fluid transition around 23 °C (Marsh, 1990). However, at physiological pH value, but low ionic strength, DMPG exhibits a very unusual thermal profile, with a main transition that extends over more than 15 °C. Its DSC trace displays a cooperative peak at the onset of the main transition ( $T_m^{on} \sim 17$  °C), followed by a broad set of peaks, and frequently a final small peak ( $T_m^{off} \sim 35$  °C) which sets the end of the gel–fluid transition (Salonen et al., 1989; Riske et al., 1997, 1999; Heimburg and Biltonen, 1994). We shall refer to the temperature interval between  $T_m^{on}$  and  $T_m^{off}$  as the *transition region*, since it separates the gel and fluid phases. Clearly, the electrostatic

\* Corresponding author. Tel.: +55 11 3091 6829; fax: +55 11 3813 4334.  
E-mail address: [mtlamy@if.usp.br](mailto:mtlamy@if.usp.br) (M.T. Lamy).

repulsion between charged PG<sup>-</sup> groups at low ionic strength determines this peculiar behavior of DMPG dispersions.

Along the DMPG *transition region* observed for low ionic strength samples the aqueous dispersion shows low turbidity (Heimburg and Biltonen, 1994), high electrical conductivity (Riske et al., 1997; Barroso et al., 2010) and high viscosity (Heimburg and Biltonen, 1994; Barroso et al., 2010; Schneider et al., 1999; Duarte et al., 2008). The structure of DMPG aggregates within the *transition region* is still a matter of debate. Because of the high viscosity of DMPG dispersions in the *transition region*, and on the basis of cryo-transmission and freeze-fracture electron microscopy data, it was proposed some time ago that DMPG at low ionic strength forms a lipid network, similar to the so-called sponge phase (Schneider et al., 1999). However, this possibility was ruled out on the basis of experiments that discarded lipid exchange between DMPG structures within the *transition region* (Lamy-Freund and Riske, 2003; Alakoskela and Kinnunem, 2007). It was shown that there is no fusion between DMPG aggregates along temperature variations across the *transition region* from the gel to the fluid phase and back, hence whatever lipid aggregate is present at a certain temperature in the gel (or fluid) phase it will be present along the whole range of studied temperatures, from 5 to 50 °C, in spite of possible change of form. Recently, it was shown that at low ionic strength DMPG lipids are organized as vesicles, both in the gel and in the fluid phases, albeit the experiment also established the leaky nature of those vesicles, as compared to DMPC (Barroso et al., 2012).

Along the DMPG *transition region*, it has been proposed by some of us that the lipid aggregate might be structured as perforated vesicles (Riske et al., 2004, 2009a, 2009b; Alakoskela et al., 2010). Electron spin resonance (ESR) of a spin label located at the bilayer center revealed the coexistence of two structurally different microenvironments within the DMPG *transition region*, one corresponding to a more rigid environment (gel bilayer) while the second is more fluid and more hydrated, compatible with lipids at the edges of bilayer pores (Riske et al., 2003). Small angle X-rays scattering (SAXS) revealed the presence, in the *transition region*, of a mesoscopic correlation around 370 Å which could be due to in-plane correlated pores (Riske et al., 2004). Moreover, compounds which enhance positive curvatures in lipid monolayers were shown to extend the DMPG temperature *transition region* to higher temperatures. Considering that the rims of the holes in bilayers are positive curvature structures, those experiments were discussed as indicative of the presence of perforated vesicles along the *transition region* (Alakoskela et al., 2010). The low optical turbidity of DMPG dispersions within that region (Heimburg and Biltonen, 1994), as well as the loss of optical contrast of giant DMPG vesicles in the same temperature interval (observed by optical microscopy; Riske et al., 2004) are also in accord with the presence of bilayer pores, which would decrease the contrast between the refractive indexes of the bilayer and the solvent (Disalvo, 1991; Yi and MacDonald, 1973).

The presence of bilayer pores should imply an expansion of DMPG vesicles along the *transition region*, in order to accommodate holes (Alakoskela et al., 2010). Nonetheless, in contradiction to the hole vesicle hypothesis which would explain the data from ESR, X-ray, and light scattering, dynamic light scattering (DLS) data indicated a considerable decrease of the z-average vesicle diameter within that temperature region (Alakoskela and Kinnunem, 2007).

In order to shed light on the above question, we have further probed the structure of DMPG aggregates in low ionic strength medium, through careful investigations of the aqueous lipid dispersion at different temperatures, through static and dynamic light scattering (SLS and DLS, respectively). In the case of SLS, the Zimm formalism allows the calculation of average values for the scattering particle radius of gyration ( $R_g$ ), molecular weight ( $M_w$ ), and the dispersion second virial coefficient ( $A_2$ ), which depends on

particle–particle and particle–solvent interactions (Zimm, 1948). Through DLS, the autocorrelation function of the intensity of the scattered light may be analyzed, yielding the translational diffusion coefficient of the scattering center. Thus, an effective hydrodynamic radius can be calculated under assumptions on the form of the scattering particle through the Stokes–Einstein equation.

In the present work, highly charged DMPG vesicles in low ionic strength medium were studied by SLS and DLS, at different temperatures. For comparison, the same experiments were performed on dispersions of the well-behaved zwitterionic lipid DMPC.

## 2. Materials and methods

### 2.1. Chemicals and reagents

DMPG (1,2-dimyristoyl-sn-glycero-3-[phospho-rac-glycerol] sodium salt) and DMPC (1,2-dimyristoyl-sn-glycero-3-[phosphocholine]) were from Avanti Polar Lipids (Birmingham, AL, USA), and used without further purification. HEPES (4-(2-hydroxyethyl)-1-piperazineethanesulfonic acid), EDTA (ethylenediaminetetraacetic acid disodium salt) and SDS (sodium dodecyl sulfate) were obtained from Sigma–Aldrich (St Louis, MO, USA). Polystyrene nanospheres (46 nm diameter) were from Duke Scientific Corporation (Palo Alto, CA, USA). Milli-Q Plus water (Millipore) was used throughout.

### 2.2. Lipid dispersion preparation

Lipids were dissolved in chloroform, and the solution dried under a stream of N<sub>2</sub>, forming a lipid film at the bottom of the tube. The film was left under low pressure for about 3 h to remove all traces of organic solvent. Dispersions were prepared by the addition of HEPES buffer (10 mM + 1 mM EDTA, pH 7.4), followed by vortexing for 2 min above the lipid gel–fluid transition temperature for DMPC ( $T_m = 23$  °C) or  $T_m^{off}$  for DMPG (the end of the gel–fluid transition,  $T_m^{off} \sim 35$  °C). Extruded lipid dispersions were used immediately after preparation, to avoid the formation of a lamellar crystal phase observed for DMPG samples incubated at low temperatures (Kodama et al., 1999).

When dispersed in aqueous medium, DMPC forms large multilamellar vesicles which precipitate in a short period of time (minutes). Hence, for light scattering measurements, it is necessary to work with extruded dispersions. Moreover, extrusion minimizes polydispersity, a great problem in the analysis of light scattering data. DMPC dispersions were extruded through polycarbonate filters (mini-extruder by Avanti Polar Lipids, 19 mm membranes with 100 nm pores, from Whatman plc, Maidstone, Kent, UK) till the dimensions of the particles were found to remain unchanged by DLS (31 times). Though DMPG vesicles do not precipitate, the same procedure was used, to reduce the dispersion polydispersity. Both DMPC and DMPG dispersions were found to be stable along the time of the experiment, considering DSC, DLS and SLS. Samples with different lipid concentrations were prepared by dilution of the more concentrated sample (2.5 mM, diluted to 2.0, 1.5, 1.0 and 0.5 mM, before extrusion). Accurate lipid concentrations of extruded samples were determined by phosphate analysis, according to Rouser et al. (1970). Extruded vesicles were found to be unilamellar by SAXS (small angle X-ray scattering).

### 2.3. Differential scanning calorimetry

Calorimetric measurements were carried out with a Microcalorimeter (Microcal VP-DSC, Northampton, MA, USA). Samples were heated from 5 to 50 °C at a scan rate of 20 °C/h (this condition was tested in previous works, e.g., Barroso et al., 2010).

Baseline subtractions and peak integrals were performed using the MicroCal Origin software with the additional module for DSC data analysis provided by MicroCal, as described elsewhere (Rishe et al., 2009a, 2009b). Scans shown here are typical scans obtained from three different preparations of DMPC and DMPG, extruded and non-extruded. For a given sample, very similar DSC profiles were obtained for at least the first three heating scans.

## 2.4. Light scattering

Light scattering measurements were performed with Brookhaven Instruments (Holtsville, New York, USA): a BI-200S goniometer, a BI-9000AT digital correlator, a BI-9025AT photo-multiplier and a He-Ne laser ( $\lambda = 632.8$  nm). Zimm Plot and auto-correlator control softwares were used (BI-ZPW and 9KDLSW, respectively). The sample 25 mm diameter scintillation vial was kept inside a vat containing the refractive-index-matching liquid decahydronaphthalene (decalin) (Sigma Chemical, St Louis, MO, USA), and the temperature was controlled by a circulating water bath (Poly Science, Illinois, USA). A thermocouple (Fulke, Illinois, USA) inside the decalin vat monitored the sample temperature. For each sample, static light scattering (SLS) and dynamic light scattering (DLS) measurements were performed at least twice at different scattering angles, within the range of  $40^\circ < \theta < 140^\circ$ .

Depolarized light scattering measurements were performed with a polarizer from RT-Polarization Rotators (Melles Griot, NY, USA).

### 2.4.1. SLS analysis

The Zimm approximation (Zimm, 1948) was used for analyzing the intensity of the scattered light at different angles:

$$\frac{Kc}{\Delta R_\theta} = \left( \frac{1 + R_g^2 q^2}{3} \right) \left( \frac{1}{M_w + 2A_2 c} \right), \quad (1)$$

The Rayleigh ratio ( $\Delta R_\theta$ ) is the measured excess light intensity scattered at a given scattering angle  $\theta$ , normalized to the scattered intensity of a standard solvent (benzene), the lipid concentration,  $c$ , is in mg/mL, and  $K$  is an optical constant, for vertically polarized light, given by:

$$K = \frac{4\pi^2 n^2 (dn/dc)^2}{N_A \lambda^4}, \quad (2)$$

$N_A$  is Avogadro's number,  $n$  is the solvent refractive index, and  $dn/dc$  is the dispersion refractive index increment.  $dn/dc$  values were measured with a differential refractometer (Brookhaven, Holtsville, NY, USA), using different lipid concentrations. As usual, the magnitude of the scattering vector is given by the equation  $q = 4\pi n/\lambda \sin(\theta/2)$ , where  $\lambda$  is the vacuum laser wavelength ( $\lambda = 632.8$  nm).

The first factor on the right-hand side of Eq. (1) comes from the form factor expansion, for which the radius of gyration  $R_g$  is defined as:

$$R_g^2 = \frac{1}{2N^2} \sum_i \sum_j (\bar{r}_i - \bar{r}_j)^2 \quad (3)$$

where  $\bar{r}_i$  and  $\bar{r}_j$  locates two segments of a particle divided into  $N$  equal segments. The vesicle external radius,  $R_{eff}$ , may be obtained from the radius of gyration,  $R_g$ , under the assumption of spherical vesicles, through the following relation:

$$R_g^2 = \left( \frac{3}{5} \right) R_{eff}^2 \frac{(1 - (1 - 2d/R_{eff})^5)}{(1 - (1 - 2d/R_{eff})^3)}, \quad (4)$$

where  $2d$  is the bilayer width.

For the gel phase of both DMPC and DMPG, the values for the bilayer width were  $2d_{gel}^{DMPC} = 2d_{gel}^{DMPG} = 4.24$  nm (Marsh, 1990). For the fluid phase, used values were  $2d_{fluid}^{DMPC} = 3.52$  nm and  $2d_{fluid}^{DMPG} = 3.14$  nm (obtained from Kucerka et al., 2011 and Pan et al., 2012, at  $50^\circ$  C and high ionic strength). Average values of  $2d_{transition\ region}^{DMPC} = 3.88$  nm and  $2d_{transition\ region}^{DMPG} = 3.69$  nm  $2d$  were used for the DMPC and DMPG melting regime, respectively.

The second term on the right-hand side of Eq. (1) comes from the expansion of the structure factor. In the limit of very low scattering angles and for dilute dispersions, it is possible to write it as a function of the fluctuation in density, which can be related to the virial expansion (Hiemenz, 1984). Thus  $A_2$  corresponds to the second virial coefficient, which yields information on vesicle interactions, whereas  $M_w$  corresponds to the scattering particle molar mass.

In our study,  $M_w$  corresponds to the vesicle molar mass,  $M_w^{ves}$ . Under specific hypotheses on lipid aggregate form, a nice check on results may be done from compatibility between  $R_{eff}$  and  $M_w$ . In the case of vesicles, one can write the number of lipids per vesicle ( $N_{lip/ves}$ ) as a function of the vesicle radius ( $R_{eff}$ ) and the area per lipid ( $a$ ), through the relation:

$$N_{lip/ves} = \frac{4\pi(R_{eff}^2 - (R_{eff} - 2d)^2)}{a}, \quad (5)$$

whereas the vesicle mass may be written as:

$$m_{ves} = \frac{M_w^{ves}}{N_A} = N_{lip/ves} m_{lip} \quad (6)$$

where  $m_{lip}$  is the mass of the lipid. Consistency of data may be inspected by comparing experimental  $R_{eff}$  and  $M_w$  through the relation:

$$\frac{m_{ves}}{m_{lip}} = \frac{M_w^{ves}}{M_w^{lip}} = \frac{4\pi(R_{eff}^2 - (R_{eff} - 2d)^2)}{a}. \quad (7)$$

For the lipids under study,  $M_w^{DMPC} = 677.93$  g/mol and  $M_w^{DMPG} = 688.85$  g/mol (Avanti Polar Lipids).

In order to interpret the virial coefficient  $A_2$  in terms of inter-aggregate interactions, the term responsible for interactions in Eq. (1),  $A_2 \times c$ , must be rewritten accordingly. Interactions are described through a virial coefficient for density of interacting particles, not for the mass density of lipids,  $c$  (g/L). In the lipid dispersions used here, we should look for the coefficient of aggregate density,  $\rho_{ves} = N_{ves}/V$ , where  $N_{ves}$  is the number of vesicles in volume  $V$ . Thus, the virial contribution to the intensity of scattered light of Eq. (1) must be rewritten as (Hansen and McDonald, 2000).

$$\frac{1}{M_w^{ves}} + 2A_2 c = \frac{1}{M_w^{ves}} (1 + 2\tilde{A}_2 \cdot \rho_{ves}) \quad (8)$$

The two densities,  $\rho_{ves}$  and  $c$ , are related through:

$$c \equiv \frac{\text{mass of lipid}}{V} = \frac{m_{lip} \cdot N_{lip/ves} \cdot N_{ves}}{V} = m_{ves} \rho_{ves} = \frac{M_w^{ves}}{N_A} \rho_{ves}, \quad (9)$$

with  $m_{ves}$ ,  $m_{lip}$  and  $N_{lip/ves}$  as defined above. Thus

$$M_{ves} A_2 c = \frac{M_w^{ves} A_2 M_w^{ves}}{N_A \rho_{ves}} \equiv \tilde{A}_2 \rho_{ves}, \quad (10)$$

which yields the definition for the virial coefficient for inter-aggregate interaction,  $\tilde{A}_2$ , as:

$$\tilde{A}_2 \equiv A_2 \frac{M_w^{ves}}{N_A} \quad (11)$$

Some interpretation from theory may be given to the inter-vesicles interaction coefficient  $\tilde{A}_2$ . In the case of purely excluded volume interactions, one has (Hansen and McDonald, 2000):

$$\tilde{A}_2^{th,excl} = \left(\frac{16}{3}\right) \pi R_{eff}^3, \quad (12)$$

If an attractive potential is present, then

$$\tilde{A}_2^{th} = \tilde{A}_2^{th,excl} - \frac{\epsilon_2^{th,attr}}{(k_B T)}, \quad (13)$$

in which  $k_B$  is the Boltzmann constant,  $T$  is the absolute temperature, and  $\epsilon_2^{th,attr}$  depends on the specific attractive potential. If charge is involved, the situation is less clear, since the virial expansion may be inadequate (Hill, 1986). Nonetheless, the presence of interactions beyond excluded volume can be inferred by comparing experimental results with the theoretical excluded volume coefficient (Eq. (12)).

#### 2.4.2. Scattered light depolarization measurements

The polarization of the scattered light depends on the polarization of the incident light and on the scattering particle induced dipole moment,  $\boldsymbol{\mu}$ , which is a function of the incident electric field ( $\mathbf{E}$ ) according to the equation  $\boldsymbol{\mu} = \tilde{\boldsymbol{\alpha}} \mathbf{E}$ , where  $\tilde{\boldsymbol{\alpha}}$  is the particle polarizability tensor. For spherical molecules, the induced dipole moment is parallel to the incident electric field, so the polarizability is a scalar quantity,  $\alpha$ , and incident and scattered light polarizations are parallel. However, for anisotropic molecules, the polarizability is a tensor ( $\tilde{\boldsymbol{\alpha}}$ ), and the polarization of the scattered light is not parallel to that of the incident light, but strongly depends on  $\tilde{\boldsymbol{\alpha}}$ . Hence, an anisotropic molecule, or particle, significantly depolarizes the incident light (Carlson and Flory, 1977).

To evaluate the anisotropy of DMPG and DMPC vesicles, the scattered light was collected in both parallel ( $I_{VV}$ ) and perpendicular ( $I_{VH}$ ) directions with respect to the polarized direction of the incident beam ( $I_V$ ). The depolarization ratio of benzene ( $I_{VV}/I_{VH} = 0.26$ ) was used as standard, to confirm the polarizer correct position.

#### 2.4.3. DLS analysis

In DLS measurements, the autocorrelation function of the intensity of the scattered light,  $g^{(2)}(\tau)$ , is directly obtained by a digital correlator, and can be related to the electric field autocorrelation function  $g^{(1)}(\tau)$  by the Siegert relation (Berne and Pecora, 2000):

$$g^{(2)}(\tau) = \beta(1 + |g^{(1)}(\tau)|). \quad (14)$$

Here, autocorrelation functions were obtained for several angles, and  $g^{(1)}(\tau)$  analyzed by the Method of Cumulants (Koppel, 1972), which yields the relation:

$$g^{(1)}(\tau) = \exp \left\{ (-\Gamma\tau) \left[ 1 + \frac{\mu_2}{2!} \tau^2 - \frac{\mu_3}{3!} \tau^3 + \dots \right] \right\}. \quad (15)$$

where  $\mu_n$  is the  $n$ th moment of the expansion, and  $\Gamma$  is called the average decay rate or relaxation frequency.  $\Gamma$  and  $\mu_2$  were obtained from software fitting based on Eq. (15), up to second order.

$\Gamma$  is related to the z-average translational diffusion coefficient ( $D_T$ ) and the scattering angle ( $q$ ), by the relation (Berne and Pecora, 2000):

$$\Gamma = D_T q^2. \quad (16)$$

The normalized variance ( $\mu_2/\Gamma^2$ ) is a measure of the system polydispersity, related to the width of the decay rate distribution.  $D_T$  values were obtained from DLS measurements at several scattering angles. For all systems studied (DMPG and DMPC dispersions at different concentrations and temperatures) rather good linear fittings were obtained for  $\Gamma \times q^2$ , as illustrated in Fig. 1.

To reduce the effect of particle–particle interaction on the calculated diffusion coefficient ( $D_T$ ), various lipid concentrations ( $c$ , in

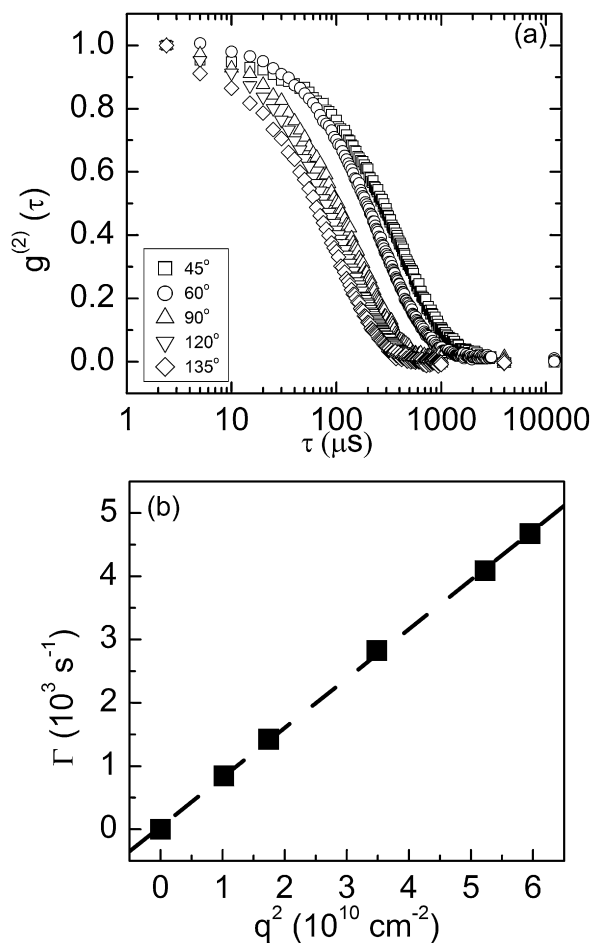


**Fig. 1.** (a) Normalized autocorrelation functions (scattered light intensity) of DMPG dispersion at 16°C (gel phase), at different scattering angles: 45°, 60°, 90°, 120° and 135°. (b) The relaxation frequency ( $\Gamma$ ) (obtained by the method of Cumulants, second order) vs. the square of the scattering vector ( $q$ ). The translational diffusion coefficient ( $D_T$ ) is calculated from the slope of the data linear fitting.

$g/L$ ) were used, and a diffusion coefficient at infinite dilution ( $D_0$ ) was calculated, according to:

$$D_T = D_0(1 + k_D c), \quad (17)$$

As the constant  $k_D$  is related to interactions in the diffusion process (Brown, 1993), this equation has been interpreted as a virial expansion (Berne and Pecora, 2000). Linear fittings of  $D_T \times c$  were obtained, and a typical plot is shown in Fig. 2.

The scattering particle dimensions may be obtained in terms of an effective hydrodynamic radius ( $R_{eff}^{(DSL)}$ ) from the diffusion coefficient  $D_0$ , according to the Einstein equation:

$$D_0 = \frac{K_B T}{b}, \quad (18)$$

where  $b$  is the coefficient of the viscous force  $F_{visc} = -bv$ , for a given velocity  $v$  of the colloidal particle. In the case of spherical symmetry (surface radius  $R$ ), the viscous force is resultant from the integration of fluid pressure around the aggregate in motion (Landau and Lifshitz, 2010), and is proportional to the particle velocity through the relation:

$$F_{vis} = -bv = -\frac{3\eta}{2R} v \int ds, \quad (19)$$

where  $\eta$  is the solvent viscosity and  $\int ds$  is an integral over the spherical particle surface.

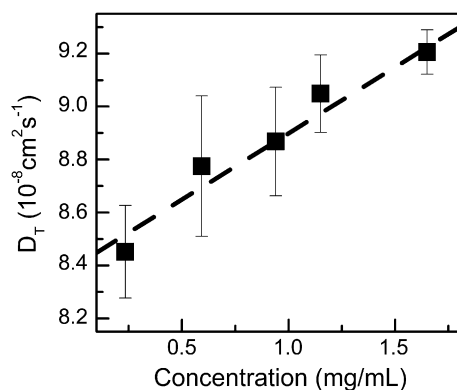


**Fig. 2.** Translational diffusion coefficient ( $D_T$ ) vs. lipid concentration, for DMPG at 28 °C (bilayer transition region). The intercept gives the diffusion coefficient at infinite dilution ( $D_0$ ), and the slope gives the concentration coefficient ( $k_D$ ).

In the case of a continuous spherical surface of radius  $R$ ,  $\int ds = 4\pi R^2$ , which yields  $b = 6\pi\eta R$ , leading to the usual Einstein–Stokes relation  $D_0 = k_B T / (6\pi\eta R)$  and to the possibility of determining the hydrodynamic radius from the diffusion constant obtained from experimental data through

$$R_{eff} = \frac{k_B T}{6\pi\eta D_0}. \quad (20)$$

We shall review the interpretation of this expression in the next section.

### 3. Results and discussions

#### 3.1. Differential scanning calorimetry

Considering that extruded dispersions of DMPG and DMPC were used (see Section 2), their DSC traces were obtained to be compared with the well-known DSC traces of non-extruded lipids (see, for instance, Barroso et al., 2010). Despite small differences, extruded DMPG dispersion, at low ionic strength, displays the characteristic complex calorimetric profile as non-extruded ones (Fig. 3). For extruded vesicles, the pre-transition is less evident and shifted to higher temperatures (from around 10 °C to 12 °C), and the peak that characterizes the onset of the main transition ( $T_m^{on}$ ) is clearly diminished as compared with the other thermal events (at least two broad peaks at higher temperatures, and a third that characterizes the end of the transition region,  $T_m^{off}$ , at around 37 °C). The heat capacity variation over the transition region was found to decrease to ~75% of its value before extrusion.

For comparison, DSC traces of extruded and non-extruded DMPC dispersions are also displayed in Fig. 3. As shown before (Ivanova and Heimburg, 2001), with extrusion, the DMPC pre-transition disappears, and the main transition becomes less cooperative (a broader peak around 23 °C). The latter effect was attributed to the increase in bilayer curvature, hence a decrease in lipid–lipid interaction. Accordingly, the variation of the heat capacity along the gel–fluid transition was found to decrease to around 90% of its original value.

Static and dynamic light scattering (SLS and DLS, respectively) at different scattering angles, from 40° to 140°, were performed for extruded DMPG in the gel (16 °C; here it will be called gel phase, though it is after a small thermal event, possibly a pre-transition, see Fig. 3) and fluid (43 °C) phases, and within the transition region (20 and 28 °C). Extruded DMPC was monitored before the main transition (20 °C; gel phase), at 23 °C, which is the beginning of the transition for extruded vesicles (see Fig. 3), and at the fluid phase (43 °C).

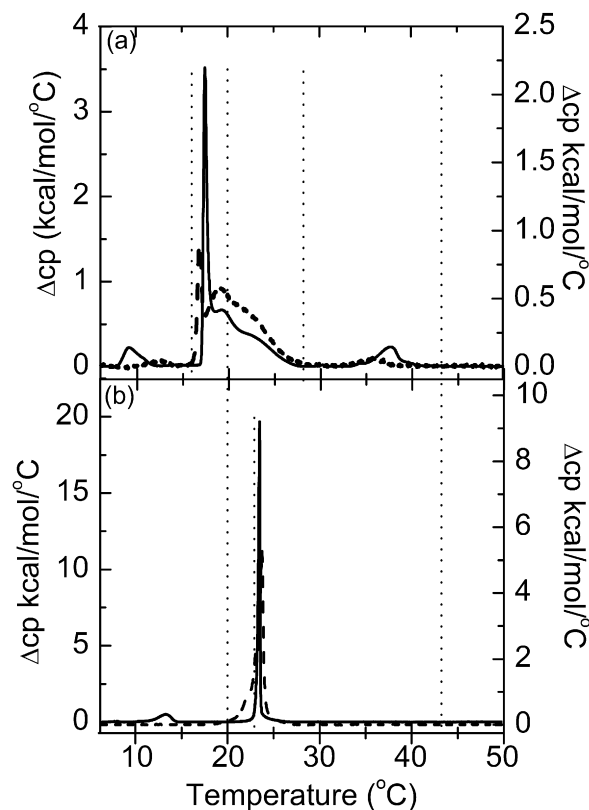


**Fig. 3.** Typical DSC heating scans of DMPG (a) and DMPC (b) dispersions (1 mM), non-extruded (solid line, left scale) and extruded (dashed line, right scale). Dotted lines indicate temperatures at which light scattering measurements were carried out.

#### 3.2. Static light scattering

Fig. 4 shows typical angular variations of the intensity of scattered light for DMPG and DMPC at different temperatures. It is interesting to note that there is a strong dependence of the scattered light intensity ( $\Delta R_\theta$ ) on the scattering angle for DMPG along the transition region (20 and 28 °C), though the scattered intensity is significantly lower (larger values of  $1/\Delta R_\theta$ ) (Fig. 4a), in accordance with previous results (see, for instance, Riske et al., 1997). As expected, gel phase bilayers of DMPG (16 °C) and DMPC (20 and 23 °C) scatter more light than fluid membranes (43 °C), a feature which has been attributed to the higher refractive index of gel membranes, as compared with fluid ones (Disalvo, 1991; Yi and MacDonald, 1973). As can be seen from the figure, the scattering angle dependence is similar for both gel and fluid phases of the same lipid, with DMPC showing a slightly stronger light scattering angular dependence. As discussed below, a stronger dependence of the intensity of the scattered light on the scattering angle may be interpreted, according to the Zimm approximation we use, to larger particle dimensions.

Two sets of four different lipid concentrations, from 0.5 to 2.5 mM (concentrations were rigorously calculated, see Section 2), were used for the Zimm analyses of both DMPG and DMPC dispersions. Very good fittings were found for all Zimm plots. Fig. 5 shows typical Zimm plots for DMPG at 28 °C (at the transition region) and DMPC at 23 °C (beginning of the melting process).

In Table 1 we present vesicle properties obtained from Zimm plots. From those plots,  $z$ -average values for the radius of gyration ( $R_g$ ) and the second virial coefficient ( $A_2$ ) can be obtained in the  $c \rightarrow 0$  and  $q \rightarrow 0$  limits, respectively, as can be seen from Eq. (1). Values for the weight-average molecular weight ( $M_w$ ) can also be

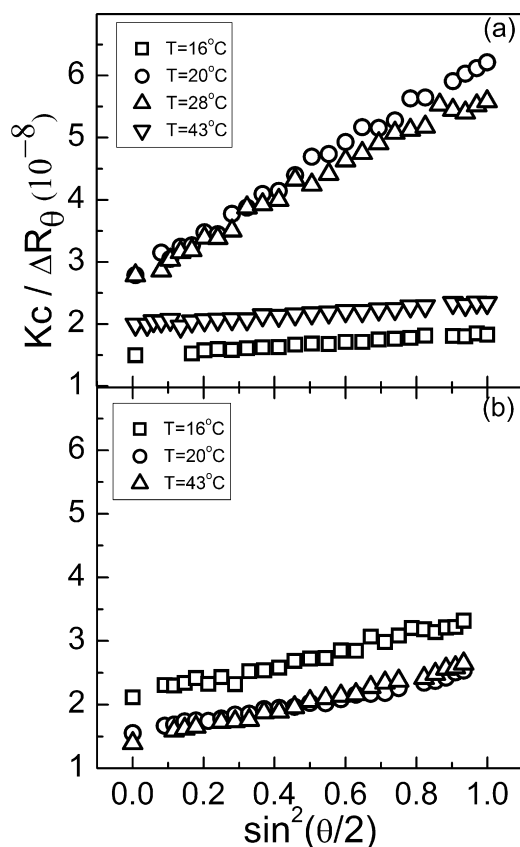


**Fig. 4.** The Rayleigh ratio ( $\Delta R_\theta$ ) dependence on the scattered angle ( $\theta$ ), for DMPG (0.60 mM) (a) and DMPC (0.55 mM) (b) dispersions, at different temperatures. DMPG at 16 °C (□, gel phase), 20 and 28 °C (○ and △, respectively, *transition region*), and 43 °C (▽, fluid phase); DMPC at 20 °C (□, gel phase), 23 °C (○, beginning of the phase transition) and 43 °C (△, fluid phase) (see Fig. 3).

obtained, by extrapolating the data to both zero angle and zero concentration. Numbers shown are averages obtained from two different Zimm plots (two sets of samples). Additionally,  $M_w$  values are averages obtained by extrapolating the data to both zero angle and zero concentration.

Values of  $M_w$ ,  $A_2$  and  $R_g$  are averages (with standard deviations) obtained from two different Zimm plots (two sets of samples). Moreover,  $M_w$  values are averages obtained by extrapolating the data to both zero angle and zero concentration.  $R_{eff}^{(SLS)}$  values were obtained from  $R_g$  values through Eq. (4) (see Section 2).  $R_{eff}^{(DLS)}$  values were obtained from diffusion constant  $D_0$  under the assumption of continuous spherical surface (Eq. (20)).

**Table 1**

Weight-average values of the vesicle molecular weight ( $M_w$ ), and z-average values of the second virial coefficient ( $A_2$ ) and the vesicle radius of gyration ( $R_g$ ) obtained from Zimm plots (Eq. (1)), at different temperatures, for DMPG and DMPC dispersions.

$T$ (°C)	SLS			DLS	
	$M_w$ ( $10^7$ g/mol)	$A_2$ ( $10^{-6}$ cm <sup>3</sup> mol/g <sup>2</sup> )	$R_g$ (nm)	$R_{eff}^{(SLS)}$ (nm)	$R_{eff}^{(DLS)}$ (nm)
<b>DMPG</b>					
16	4.9 ± 1.5	3.7 ± 1.6	30 ± 4	31 ± 3	24 ± 1
20	4.1 ± 0.8	8 ± 3	77 ± 4	78 ± 3	29 ± 1
28	4.8 ± 1.2	11 ± 4	89 ± 3	92 ± 5	32 ± 1
43	6.5 ± 2.3	3.1 ± 1.5	33 ± 4	34 ± 4	28 ± 3
<b>DMPC</b>					
20	6.5 ± 1.4	3.5 ± 1.4	51 ± 2	54 ± 1	53 ± 4
28	8.7 ± 1.3	4.0 ± 0.3	51 ± 2	53 ± 2	53 ± 4
43	9 ± 2	2.0 ± 1.3	61 ± 1	62 ± 2	60 ± 5

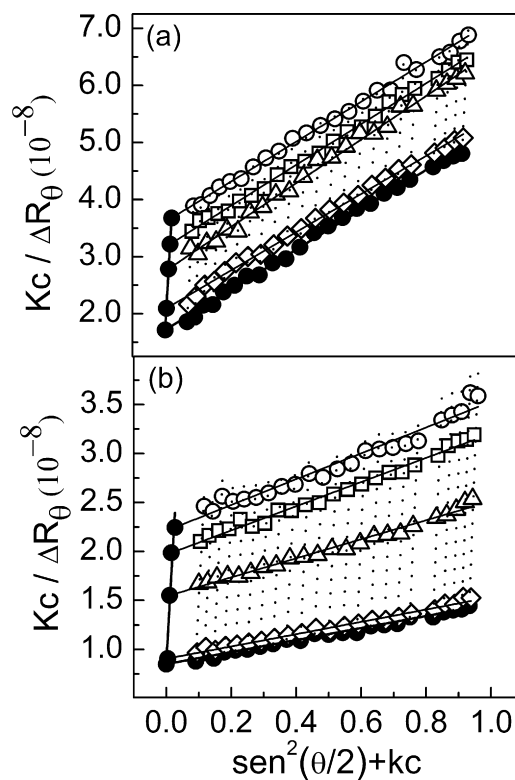


**Fig. 5.** Typical Zimm plots obtained for dispersions of DMPG at 28 °C (*transition region*) (a) and DMPC at 23 °C (beginning of the phase transition) (b). DMPG concentrations: 0.214 mM (◇), 0.579 mM (△), 1.160 mM (□), and 1.640 mM (○). DMPC concentrations: 0.285 mM (◇), 0.590 mM (△), 0.895 mM (□), and 1.566 mM (○).

The new feature shown by our data is the huge increase in DMPG vesicle size within the *transition region*:  $R_g$  suffers a threefold increase from around 30 nm at 16 °C, in the gel phase, to 90 nm at 28 °C, well inside the *transition region* (Fig. 3). Also, an increment in size can be noticed inside the *transition region* itself, as  $R_g$  is higher at 28 °C than at 20 °C.

Such a large increase in the radius of vesicles requires rationalization, which must take into account previous studies based on ESR and fluorescent probes experiments (Lamy-Freund and Riske, 2003; Alakoskela and Kinnunen, 2007) which have demonstrated the *absence of fusion* of DMPG vesicles along the *transition region*.

Table 1 displays the effective radii ( $R_{eff}^{(SLS)}$ ) for both DMPG and DMPC, at different temperatures.  $R_{eff}^{(SLS)}$  values were calculated under the assumption of spherical unilamellar vesicles from Eq. (4) (see Section 2), from the radius of gyration  $R_g$  yielded by Zimm plots, in accordance with Eq. (1). For DMPC, calculations yielded

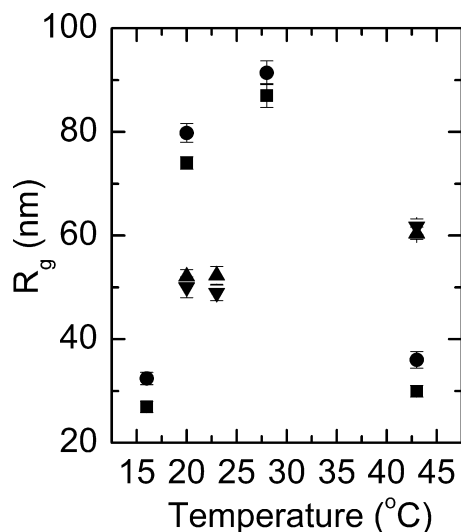


Fig. 6. Temperature dependence of the radius of gyration of DMPG (■ and ●, from two different Zimm plots, Eq. (1)) and DMPC (▲ and ▼, from two different Zimm plots, Eq. (1)) vesicles.  $R_g$  values were obtained from Zimm plots (Eq. (1)).

radii close to expected values, considering that dispersions were filtered through 100 nm pore filters: ~54 nm for the gel phase (20 and 23 °C) and ~62 nm for the fluid phase (43 °C). Surprisingly, the diameters of the DMPG vesicle were found to be much smaller than the filter pore size, both in the gel and in the fluid phases, since effective radii of 31 and 34 nm were found for the two “normal” lipid phases, respectively (Table 1). This strongly indicates the presence, before extrusion, of a large amount of aggregates smaller than the filter pore size (100 nm) in DMPG dispersions. It is important to note that no significant amount of micelles or bicelles are present in DMPG dispersions, as indicated by the ESR signal of spin labels incorporated into the lipid aggregate (Barroso et al., 2012).

In Table 1 we also present weight-average aggregate molecular weight values ( $M_w$ ) obtained from Eq. (1) at both limits,  $c \rightarrow 0$  and  $q \rightarrow 0$ , for both DMPG and DMPC at different temperatures. The numbers (average values) and corresponding deviations were obtained from two sets of experiments and from the two extrapolation procedures. It can be seen that, within error bars, the aggregate molecular weight does not change. Hence, in spite of the dramatic increase of  $R_g$  over the DMPG transition region (Fig. 6), the vesicle molecular weight remains nearly unchanged, as expected from the absence of fusion demonstrated in other experimental procedures (Lamy-Freund and Riske, 2003; Alakoskela and Kinnunen, 2007).

The consistency between results for aggregate radius and mass can be checked (Eq. (7)). For instance, in the case of DMPG, assuming unilamellar vesicles with  $R_{eff}^{(SLS)} \sim 31$  nm for the gel phase (Table 1), area per lipid headgroup  $\sim 0.48$  nm<sup>2</sup> (Marsh, 1990), and lipid molecular weight  $M_w^{DMPG} = 689$  g/mol, one obtains  $M_w^{ves,DMPG} \sim 3.0 \times 10^7$  g/mol. Similar calculations for DMPC in the gel phase, with  $R_{eff}^{(SLS)} \sim 54$  nm (Table 1), and  $M_w^{DMPC} = 678$  g/mol, yield  $M_w^{ves,DMPC} \sim 9.6 \times 10^7$  g/mol. As can be seen from the table, data obtained for  $M_w$  are in good agreement with effective radii  $R_{eff}^{(SLS)}$ , giving good reliability to our results on aggregate size and stability of the DMPG aggregates across the transition region.

In relation to inter-vesicle interactions,  $A_2$  values were found to be positive, both for DMPC and for DMPG, indicating dominance of repulsive interactions between vesicles, as shown in Fig. 7 and Table 1. On average, for gel and fluid vesicles, DMPG values are somewhat higher than those obtained for DMPC. However, along the DMPG transition region,  $A_2$  increases approximately 4 times (at 28 °C) as compared to the value at the gel phase.

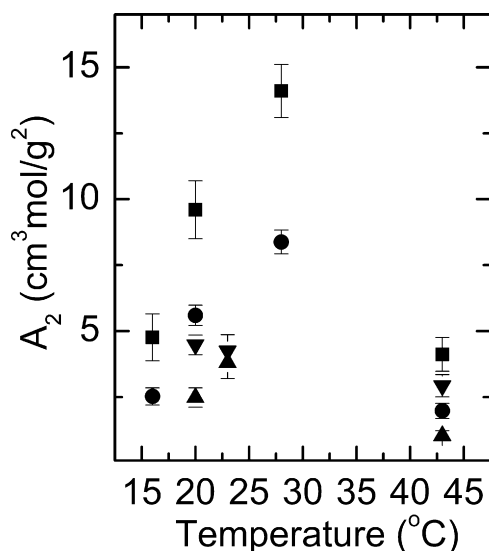
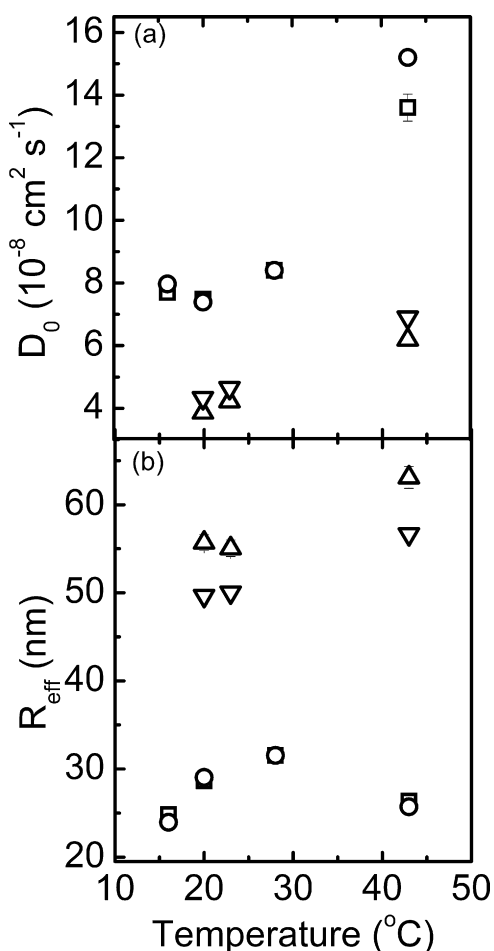


Fig. 7. Temperature dependence of the second virial coefficient ( $A_2$ ) of DMPG (■ and ●, from two different Zimm plots, Eq. (1)) and DMPC (▲ and ▼, from two different Zimm plots, Eq. (1)) dispersions, obtained from Zimm plots (Eq. (1)).

In order to give some physical interpretation for the differences in  $A_2$  values for the two lipid dispersions, we compare the inter-particle virial coefficients  $\tilde{A}_2$  for the two systems (see Eqs. (10) and (11)). First we examine the virial coefficient for neutral DMPC. From Table 1, we have for the experimental ratio  $\alpha_{exp} \equiv \tilde{A}_2^{(gel)} / \tilde{A}_2^{(fluid)} \approx A_2^{(gel)} / A_2^{(fluid)} \approx 1.8$ , whereas from Eq. (12), we would have for excluded volume interactions the theoretical ratio  $\alpha_{th,excl} \equiv \tilde{A}_2^{(gel,excl)} / \tilde{A}_2^{(fluid,excl)} \approx (R_{eff}^{(SLS,gel)} / R_{eff}^{(SLS,fluid)})^3 \approx 0.7$  ( $R_{eff}^{(SLS)}$  from Table 1). The experimental result may be rationalized only in terms of Eq. (13), which adds attractive interactions to the excluded volume model, with the attractive interaction between vesicles increasing in the fluid phase. Comparison of the virial coefficients for the two “normal” phases of DMPG yields a similar picture, with  $\alpha_{exp} \equiv \tilde{A}_2^{(gel)} / \tilde{A}_2^{(fluid)} \approx A_2^{(gel)} / A_2^{(fluid)} \approx 1.2$  from experimental values (Table 1), and  $\alpha_{th,excl} \equiv \tilde{A}_2^{(gel,excl)} / \tilde{A}_2^{(fluid,excl)} \approx (R_{eff}^{(SLS,gel)} / R_{eff}^{(SLS,fluid)})^3 \approx 0.7$  ( $R_{eff}^{(SLS)}$  from Table 1) for the theoretical ratio. The discrepancy between theoretical and experimental ratios is smaller for DMPG than for DMPC, which might imply a smaller attractive contribution for DMPG negatively charged vesicles (see Eq. (13)). However, if we compare DMPG virial coefficients of the transition region and of the fluid phase, for instance, the discrepancy between theory and experiment seems to go in the opposite direction:  $\alpha_{th,excl} \equiv \tilde{A}_2^{(trans.,28)} / \tilde{A}_2^{(fluid,43)} \approx A_2^{(trans.,28)} / A_2^{(fluid,43)} \approx 3.6$  and  $\alpha_{th,excl} \equiv (R_{eff}^{(SLS,trans)} / R_{eff}^{(SLS,fluid)})^3 \approx 19$  (see Table 1). The theoretical value is much larger than the experimental one. Could this be explained in terms of vesicle charging in the transition region (Barroso et al., 2010; Henriques et al., 2011)? The answer to this question demands new theoretical developments, not given in this study.

### 3.3. Dynamic light scattering

DLS measurements were carried out at the same temperatures and lipid concentrations used for SLS. As mentioned in Section 2, translational diffusion coefficients ( $D_T$ ) were obtained from DLS measurements at several scattering angles, and translational diffusion coefficients at infinite dilution ( $D_0$ ) were calculated according to Eq. (17). For DMPC, the expected increase of  $D_0$  values with temperature was observed (Fig. 8a). However, for DMPG, a clear anomaly is observed in the transition region (20 and 28 °C).



**Fig. 8.** Temperature dependence of the diffusion coefficient at infinite dilution (a) and the effective radius  $R_{\text{eff}}^{\text{DLS}}$  (b), for DMPG ( $\square$  and  $\circ$ , from two sets of samples with different lipid concentrations) and DMPC ( $\triangle$  and  $\nabla$ , from two sets of samples with different lipid concentrations) vesicles.

Fig. 8b shows effective radius obtained from diffusion coefficients, if continuous surface spherical vesicles are assumed, as in the Stokes–Einstein equation (Eq. (20)). Such an analysis of DLS leads to an increase in vesicle size along from the gel to the fluid phase, in accordance with the results of SLS experiments (see Table 1). However, results for the DMPG *transition region* obtained through the two techniques are very different: if gel phase data (at  $16^{\circ}\text{C}$ ) are compared to *transition region* data (at  $28^{\circ}\text{C}$ ), the increase in  $R_{\text{eff}}$  is almost threefold in the case of SLS, while for DLS we find a bare 30% increase (see  $R_{\text{eff}}^{\text{SLS}}$  and  $R_{\text{eff}}^{\text{DLS}}$  in Table 1). The possible origin of this important discrepancy lies in the assumptions used in the interpretation of the raw data, as we discuss in the next section.

Calculated normalized variances ( $\mu_2/\Gamma^2$ ), related to the system polydispersity (Berne and Pecora, 2000), indicate an increase in the polydispersity along the DMPG *transition region*, as compared with gel and fluid phases of DMPG and DMPC (Table 2). It is also interesting to note that the concentration coefficient  $k_D$  (Eq. (17)), which is an indication of vesicle–vesicle interaction (Berne and Pecora, 2000) is larger for DMPG than for DMPC dispersions, and, for DMPG, larger values were obtained at  $28^{\circ}\text{C}$  (Table 2). This is similar to the behavior observed for the second virial coefficient  $A_2$  (Fig. 7).

An essential point to be noted is that the results presented here for the z-average hydrodynamic radius of DMPG vesicles were obtained for *extruded* DMPG dispersions, which are drastically different from results obtained for non-extruded dispersions. Our data for the latter, not shown, are in accordance with those of

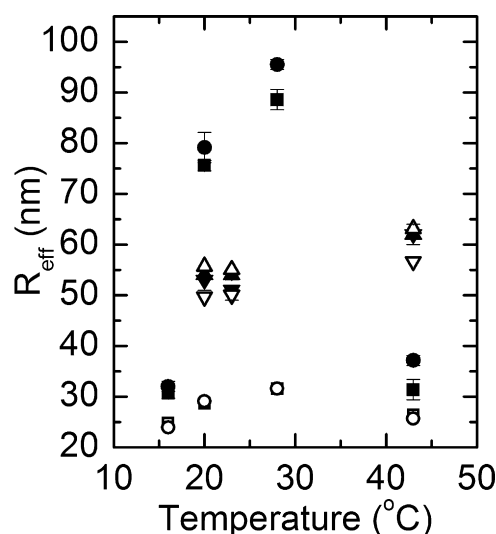


**Fig. 9.** Comparison of  $R_{\text{eff}}$  values calculated by SLS (closed symbols,  $R_{\text{eff}}^{\text{SLS}}$ ) and DLS (open symbols,  $R_{\text{eff}}^{\text{DLS}}$ ), at different temperatures, for DMPG ( $\blacksquare$ ,  $\bullet$ ,  $\square$  and  $\circ$ ) and DMPC ( $\blacktriangle$ ,  $\blacktriangledown$ ,  $\triangle$  and  $\triangledown$ ). Here results from two sets of experiments, with both techniques, are shown for the two lipid dispersions. (In Table 1, average values of  $R_{\text{eff}}^{\text{SLS}}$  and  $R_{\text{eff}}^{\text{DLS}}$  are shown).

Alakoskela and Kinnunen (2007). In the absence of extrusion, DLS indicates a *decrease* of the z-average hydrodynamic radius of DMPG vesicles within the *transition region*, whereas after extrusion, an *increase* is observed, within the same temperature range. That difference is certainly related to the high polydispersity of non-extruded samples, though the complete rationale behind it is out of the scope of the present work. A second essential point to note is that the Zimm analysis by SLS was found to be impossible for non-extruded DMPG dispersions. Hence, we are convinced that trustworthy analyses by SLS and DLS are only possible with extruded DMPG dispersions, considering that extruded dispersions display similar peculiar characteristics along the *transition region*, like the broad DSC profile (Fig. 3), low turbidity (Fig. 4), high viscosity and conductivity (results not shown).

### 3.4. Comparing SLS and DLS results

Fig. 9 displays a comparison between values obtained for  $R_{\text{eff}}$  from SLS and DLS data, and analysis  $R_{\text{eff}}^{\text{SLS}}$  and  $R_{\text{eff}}^{\text{DLS}}$  in Table 1. Results from the two techniques are in very good accordance for DMPC dispersions, strongly supporting data analyses performed here for the two techniques. In the case of DMPG, SLS analyses yield somewhat larger values than DLS ( $\sim 20\%$  larger), both for the fluid and for the gel phases. However, the huge difference in  $R_{\text{eff}}$  values obtained with the two techniques within the DMPG *transition region* poses questions on hypotheses which is based on interpretation of data.

Previous studies have established two important features of DMPG dispersions, with respect to aggregate structure. On the one hand, DMPG has been shown to organize as vesicles in the gel and fluid phases (see Barroso et al., 2012, and references therein), even at the low ionic strength used here (10 mM HEPES pH 7.4). On the other hand, no fusion of aggregates is present along the *transition region* (Lamy-Freund and Riske, 2003; Alakoskela and Kinnunen, 2007).

What, then, could be the origin of the discrepancy between results? Should our analysis take into account change of aggregate form? Could increased ionization be responsible for the lack of agreement between the two sets of interpreted data? In which way

**Table 2**  
Concentration coefficient ( $k_D$ ) and polydispersity at  $90^\circ$  ( $\mu_2/\Gamma^2$ ), for DMPG and DMPC dispersions at different temperatures.

DMPG			DMPC		
Temperature ( $^\circ\text{C}$ )	$k_D$ ( $\text{cm}^3/\text{g}$ )	Polydispersity $\mu_2/\Gamma^2$	Temperature ( $^\circ\text{C}$ )	$k_D$ ( $\text{cm}^3/\text{g}$ )	Polydispersity $\mu_2/\Gamma^2$
16	$37 \pm 16$	$0.07 \pm 0.06$	20	$12 \pm 6$	$0.09 \pm 0.02$
20	$46 \pm 22$	$0.14 \pm 0.05$	23	$10 \pm 1$	$0.07 \pm 0.02$
28	$60 \pm 2$	$0.17 \pm 0.04$	43	$30 \pm 13$	$0.10 \pm 0.03$
43	$44 \pm 9$	$0.06 \pm 0.05$			

could the perforated bilayer hypothesis be included in the analysis of data? We have investigated the answers to these questions and report on them in what follows.

### 3.5. What is the structure of DMPG vesicles along the transition region? Geometry $\times$ charge $\times$ pores

It has been suggested by different authors that the difference between effective radii calculated by SLS and DLS could be attributed to the geometry of the scattering center (Heineck et al., 2008). In order to probe possible loss of spherical geometry of the aggregate within the transition region, depolarized light scattering measurements were performed to evaluate the anisotropy of the scattering particle (see Section 2). It is known that the incident light is depolarized depending on the scattering center polarizability tensor ( $\alpha$ ), which is related to its anisotropy (Carlson and Flory, 1977). Could vesicles deform in the transition region and present aggregate anisotropy? Fig. 10 shows that the depolarization ratio ( $I_{VH}/I_{VV}$ , see Section 2) for DMPG vesicles is very low ( $\sim 0.005$ ), at all temperatures studied. More importantly, no significant increase is detected along the transition region. Moreover, the ratio  $I_{VV}/I_{VH}$  for DMPG is similar to that obtained for both DMPC and polystyrene nanospheres (46 nm diameter), indicating that DMPG forms isotropic aggregates at all temperatures. For comparison,

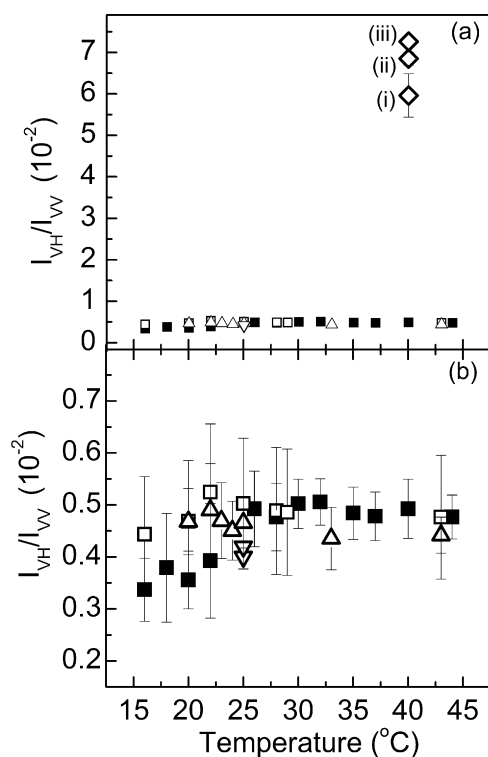


**Fig. 10.** (a) Temperature dependence of the light depolarization ratio for DMPG (■ and □ two different 1 mM samples), DMPC ( $\Delta$ , 1 mM), polystyrene spheres ( $\nabla$ ,  $\sim 1.3$  mg/mL, 46 nm diameter) and SDS ( $\diamond$ , 8.7 mM (i), 17.4 mM (ii) and 34.8 mM (iii)). (b) is (a) amplified.

Fig. 10 shows the depolarization ratio yielded by SDS micelles ( $\sim 0.07$ ), which are known to form ellipsoids at the concentrations used here ( $\sim 8.7$  mM, 17.4 mM and 34.8 mM) in water (Bergnröm and Pedersen, 1999). Thus we must conclude for spherical vesicles along the whole transition region, which discards the hypothesis of tattered open sheets over the transition region, as suggested before (Alakoskela and Kinnunem, 2007).

On the other hand, an increase in the area per lipid head-group due to electrostatic repulsion, related to the increase in vesicle ionization within the transition region for low ionic strength samples (Barroso et al., 2010) could explain an increase in the vesicle  $R_{eff}$ . However, it could not be responsible for the threefold  $R_{eff}^{(SLS)}$  increase (Table 1 and Fig. 9). The doubling of the area per lipid due to electrostatic repulsion, for instance, would yield a bare increase of  $1.4 R_{eff}$ .

Finally, how would pores modify vesicle radius? The presence of bilayer pores along the DMPG transition was proposed to explain the mesoscopic correlation detected by SAXS (Riske et al., 2004; Spinozzi et al., 2010), as well as the coexistence of two different lipid microenvironments, detected by ESR (Riske et al., 2003).

Alakoskela et al. (2010) proposed a mathematical model for the holey vesicle which yields increased radius of the perforated vesicle, depending on the number and size of holes, with preservation of the bilayer volume. A vesicle with a hole is represented in Fig. 11 below.

While holes contribute to increase the effective vesicle radius ( $R_{eff}$ ), some lipid molecules must occupy the hole rim, in order to shield the bilayer hydrophobic core. Thus, considering the preservation of the vesicle bilayer volume  $V_0$  (volume of the bilayer

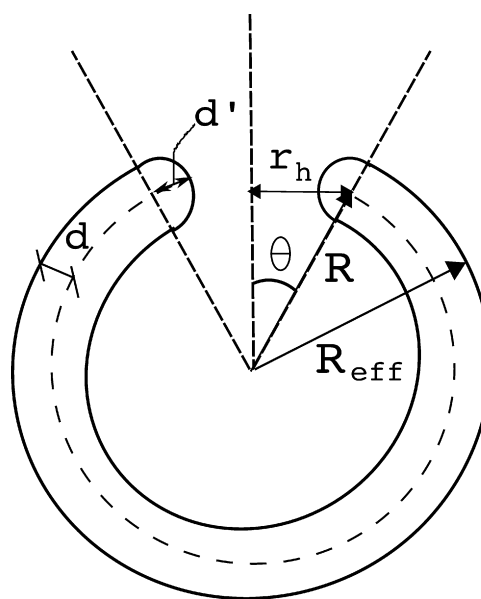


**Fig. 11.** Illustration of a section of the holey vesicle (holey spherical shell) with one pore (hole).  $R_{eff}$  is the external radius of the holey vesicle, and  $R$  is the distance from the center to the middle of the bilayer, ( $R_{eff} - d$ ),  $d$  is the bilayer half width, and  $d'$  is the rim width. The radius of the pore is given by  $r_h = R \sin \theta$ .

without perforations, in the gel or fluid phases of the lipid), for  $n$  holes, the volume of the perforated vesicle would be given by  $V_0 = V_{sph.shell} - nV_{hole} + nV_{rims}$ , where  $V_{sph.shell}$  is the volume of the enlarged vesicle in the *transition region* neglecting the holes, and  $V_{hole}$  and  $V_{rims}$  are the hole and rim volumes, respectively.

Considering the bilayer volume preservation, in the gel phase the vesicle effective radius is smaller and the bilayer width is larger than in the fluid phase. Here, an intermediate radius between the radii found by SLS for the gel and the fluid phases was used ( $R_{eff}^0 = 33$  nm, as compared with 31 and 34 nm, found for the gel and fluid phases, respectively, see Table 1), and an intermediate value for the bilayer width was calculated, so the bilayer volume was preserved as compared to the gel phase ( $d = 1.89$  nm). The rationale behind the above hypothesis is the observation that the more rigid microenvironment detected in the DMPG bilayer within the *transition region* is not as rigid as that observed for DMPG gel phase (Riske et al., 2003).

Following Alakoskela et al. (2010), we calculated the vesicle  $R_{eff}$  dependence on the number and size of bilayer holes (Fig. 12 and Supplementary Material), and compared the theoretical results with the maximum experimental value obtained for DMPG  $R_{eff}^{(SLS)}$  along the *transition region*:  $92 \pm 5$  nm at  $28^\circ\text{C}$  (Table 1), shown as dashed stripes in Fig. 12 (left scale). The case of equal lipid fluidity at pores and bilayers ( $d' = d$  in Fig. 11, see Supplementary Material) is illustrated in Fig. 12a, for different values of  $r_h$ : 10, 15 and 20 nm. It is evident from Fig. 12a that the model cannot explain the huge increase observed on  $R_{eff}^{(SLS)}$ . Also shown in Fig. 12 is the fraction of lipids in the pore rims ( $V_{rims}/V_0$ ) (right scale), which should stay well under unity.

Still considering ESR experiments (Riske et al., 2003), which showed the coexistence of two different lipid microenvironments within the DMPG *transition region*, one of them corresponding to a rather fluid and hydrated domain, attributed to lipids at pore rims, we have extended the above model, adding a new feature to it. We allowed the lipids along the rims to be less packed than those in the bilayer, which means allowing  $d' < d$  on the rims (see Supplementary Material). Fig. 12b and c shows  $R_{eff}$  theoretical results obtained making  $d' = 1.13 d_{fluid} = 1.77$  nm, and  $d' = 0.8 d_{fluid} = 1.24$  nm, respectively. The latter would be in accord with experimental results, which showed that the “fluid domain” along the *transition region* is still more fluid than a normal fluid bilayer (Riske et al., 2003).

It is very interesting to observe that if we include in the theoretical model the presence of more fluid lipids along the pores rims (Fig. 12c), the radius of the vesicle can increase considerably, easily achieving the experimental SLS values ( $92 \pm 5$  nm). Note that the left and right scales in Fig. 12 should be read for the same value of number of holes, both for  $R_{eff}$  (left scale) and for  $V_{rims}/V_0$  (right scale). For instance, in Fig. 12b, the dotted line shows that  $R_{eff} \approx 88$  nm corresponds to  $V_{rims}/V_0 \approx 0.8$ , for holes of size  $r_h = 20$  nm (huge holes); the actual radius of the hole is  $r_h - d'$ , so  $r_h^{actual} = 20 - 1.77 = 18.23$  nm, see Fig. 11). As for the very fluid rims (Fig. 12c), experimental values for  $R_{eff}$  are achieved for  $V_{rims}/V_0 \approx 0.41$ – $0.53$  for large pores (20 nm), but pore radius could also be smaller, around 10 nm ( $V_{rims}/V_0 \approx 0.8$ , Fig. 12c). Hence, highly perforated vesicles could explain the tremendous increase of vesicle radius obtained by SLS data, though even 10 nm radius pore is certainly a huge bilayer pore, which needs theoretical investigation, taking into account the balance between electrostatic and hydrophobic interactions.

It is interesting to point out that if one considers an organized lattice of pores (for instance, a vesicle with  $R_{eff} \sim 90$  nm and 70 holes), the average distance between pores (Fig. 12) would be in accord with SAXS data, around 40 nm (Riske et al., 2004; Spinozzi et al., 2010). That can be calculated by considering the area of

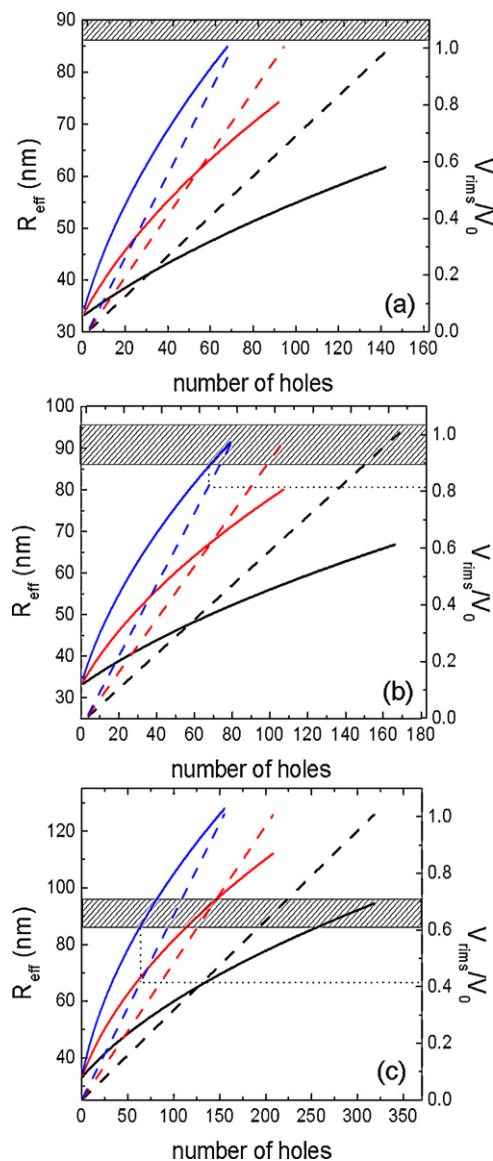


**Fig. 12.** Theoretical calculation of the effective radius of the vesicle ( $R_{eff}$ , — left scale), and the ratio between the holes rims volume and the lipid total volume ( $V_{rims}/V_0$ , ---, right scale), as a function of the number of vesicle holes (see Supporting information). Black, red and blue lines correspond to  $r_h = 10, 15$  and  $20$  nm, respectively (see Fig. 11). (a)  $d' = d = 1.89$  nm, (b)  $d' = 1.13 d_{fluid} = 1.77$  nm, (c)  $d' = 0.8 d_{fluid} = 1.24$  nm. Dashed stripes ( $R_{eff}$ , left scale) correspond to the maximum experimental value obtained for DMPG  $R_{eff}^{(SLS)}$  along the *transition region*:  $92 \pm 5$  nm, at  $28^\circ\text{C}$  (Table 1). (For interpretation of the references to color in this figure legend, the reader is referred to the web version of this article.)

the vesicle and the number of holes (distance<sup>2</sup> =  $4\pi R_{eff}^2$ /number of holes). Considering the size of the holes and the average distance between them, DMPG bilayers would be highly tattered bilayers along the lipid *transition region*.

The above calculations allow one to explain SLS results. However, how does one make them compatible with DLS results, which point to much smaller vesicles within the DMPG *transition region*? An essential point to note is that the hydrodynamic radius was calculated from the diffusion constant through the Einstein–Stokes relation (Eq. (20)), under the assumption of continuous surface for the spherical vesicle. Under the new picture, of perforated vesicles, how can the aggregate size be reinterpreted from the diffusion constant? The viscous force is resultant from the integration of fluid pressure around the aggregate in motion (Landau and Lifshitz, 2010), as discussed in Section 2. In the case of the perforated sphere,

the resisting surface is approximately the same as the surface of the integral vesicle. Thus if we consider as a first approximation that the spherical geometry for the fluid flux is maintained, with water flowing undisturbed through the pores, one would have the same resistive coefficient for both the integral and the perforated vesicles. This would explain the almost equal effective radii obtained from DLS for the fluid phase and the *transition region* (see Table 1). The diffusion constant would be almost unaffected by the transformation of the usual bilayer vesicle into a large holey vesicle. In this case, DLS would be useless in terms of probing aggregate size while the apparently contradictory result with respect to SLS would be clarified.

In line with the above discussion, it is interesting to point out the somewhat smaller  $R_{eff}$  values obtained by DLS, as compared with SLS, for DMPG vesicles even in the gel and fluid phases (Fig. 9, Table 1). That would be in accord with the observed presence of leaky vesicles in DMPG dispersions, even at low and high temperatures, 6 and 45 °C, respectively (Barroso et al., 2010).

#### 4. Conclusions

Here, freshly prepared low ionic strength DMPG dispersions were very carefully analyzed by SLS and DLS, and results compared with those obtained with dispersions of the zwitterionic lipid DMPC. For that, it was found essential to have relatively homogeneous dispersions, obtained after the extrusion process.

For DMPC, across the whole temperature range, vesicle effective radii calculated by SLS and DLS were found to be very similar, strongly supporting analyses performed here: as expected, vesicles were found to increase by around 13%, from the gel to the fluid phase.

Similar to DMPC, highly charged DMPG vesicles, in low ionic strength medium, displayed an increase in radius from the gel to the fluid phase (~15%). However, in the DMPG *transition region* (28 °C), SLS data analysis indicated a threefold increase in the vesicle dimension. DLS also indicated an increase in the vesicle effective radius, but of ~30% only. Considering that DMPG aggregates were found to have spherical geometry in the whole temperature interval, from gel to fluid phase and across the *transition region*, the huge increase in the DMPG vesicle size, detected by SLS, was interpreted in accord with the presence of highly perforated vesicles along the lipid *transition region* (Riske et al., 2004; Alakoskela et al., 2010). For a threefold increase in the vesicle effective radius it was necessary to consider that lipids in the pore rim are more fluid than those in the bilayer, in accord with previous ESR results (Riske et al., 2003).

DLS/SLS discrepancy in DMPG *transition region* is explained in terms of reinterpretation of the Einstein–Stokes relation for porous vesicles: the diffusion constant obtained by DLS is related to the radius of the resisting surface, equal to the original continuous surface, much smaller than the radius of the porous vesicle.

The above rationale may be extended to explain the low turbidity observed within the *transition region*, as the bilayer/solvent contrast would decrease due to solvent flow through bilayer pores. That would be similar, but much more drastic, to the decrease in turbidity observed at the gel–fluid transition of many bilayers (for instance, DMPC), attributed to the decrease in the refractive index contrast between the bilayer and the solvent, as fluid bilayers are more hydrated (Disalvo, 1991; Yi and MacDonald, 1973). Moreover, as discussed by Alakoskela et al. (2010), the high viscosity measured along DMPG *transition region* could be due to the huge increase in the vesicle radius, though the increase in vesicle ionization should also contribute to the increase in the dispersion viscosity (Barroso et al., 2010).

What is the physical explanation for the opening of pores in the *transition region*? Charge certainly plays a special role in that

region, as indicated by the increased conductivity displayed by the dispersion (Barroso et al., 2010; Henriques et al., 2011). Could pore formation be related to the presence of extra-charge? Could the competition between the hydrophobic force, which maintains the bilayer, be overcome by electrostatic repulsion, producing local ruptures on the bilayer? Or could an eventual imbalance of inner and outer vesicle charge trigger the process? Albeit the underlying nanoscopic process deserves further investigation, one could speculate about future biotechnological applications, with vesicles being produced to enlarge and perforate in a chosen temperature and/or pH value. For biological applications, such as drug delivery, other means to trigger pore formation at physiological ionic strength need to be developed.

#### Acknowledgments

This work was supported by USP, FAPESP and CNPq (VBH and MTL research fellowships, and TAE a M.Sc. fellowship). We are grateful to Dr. N.P. Silveira and O.N. Mesquita for interesting discussions, and to D.A. Nomura and J. Rodrigues for helping with experiments and theoretical calculations, respectively.

#### Appendix A. Supplementary data

Supplementary data associated with this article can be found, in the online version, at <http://dx.doi.org/10.1016/j.chemphyslip.2012.11.002>.

#### References

- Alakoskela, J.M., Kinnunen, P.K.J., 2007. Thermal phase behavior of DMPG: the exclusion of continuous network and dense aggregates. *Langmuir* 23, 4203–4213.
- Alakoskela, J.M., Parry, J.M., Kinnunen, P.K.J., 2010. The intermediate state of DMPG is stabilized by enhanced positive spontaneous curvature. *Langmuir* 26 (7), 4892–4900.
- Barroso, R.P., Perez, K.R., Cuccovia, I.M., Lamy, M.T., 2012. Aqueous dispersions of DMPG in low salt contain leaky vesicles. *Chemistry and Physics of Lipids* 165, 169–177.
- Barroso, R.P., Riske, K.A., Henriques, V.B., Lamy, M.T., 2010. Ionization and structural changes of the DMPG vesicle along its anomalous gel–fluid phase transition: a study with different lipid concentrations. *Langmuir* 26 (17), 13805–13814.
- Bergström, M., Pedersen, J., 1999. Structure of pure SDS and DTAB micelles in brine determined by small-angle neutron scattering (SANS). *Physical Chemistry Chemical Physics* 1, 4437–4446.
- Berne, R., Pecora, B.J., 2000. *Dynamic Light Scattering*. Dover Publications Inc., Mineola, NY, pp. 53–144.
- Brown, W., 1993. *Dynamic Light Scattering, the Methods and Some Applications*. Oxford University Press, New York.
- Carlson, C.W., Flory, P.J., 1977. Separation of collision-induced from intrinsic molecular depolarized Rayleigh scattering. *Journal of the Chemical Society, Faraday Transactions 2* (73), 1505–1520.
- Disalvo, E.A., 1991. Optical properties of lipid dispersions induced by permeate molecules. *Chemistry and Physics of Lipids* 59, 199–206.
- Duarte, E.L., Oliveira, T.R., Alves, D.S., Micol, V., Lamy, M.T., 2008. On the interaction of the anthraquinone barbaloin with negatively charged DMPG bilayers. *Langmuir* 24, 4041–4049.
- Hansen, J.P., McDonald, I.R., 2000. *Theory of Simple Liquids*, 2nd ed. London, Academic Press.
- Heimburg, T., Biltonen, R., 1994. Thermotropic behavior of dimyristoylphosphatidylglycerol and its interaction with cytochrome C. *Biochemistry* 33, 9477–9488.
- Heineck, M.E., Cardoso, M.B., Giacomelli, F.C., Silveira, N.P., 2008. Evidences of amylose coil-to-helix transition in stored dilute solutions. *Polymer* 49, 4386–4392.
- Henriques, V.B., Germano, R., Lamy, M.T., Tamashiro, M.N., 2011. Phase transitions and spatially ordered counterion association in ionic-lipid membranes: theory versus experiment. *Langmuir* 27, 13130–13143.
- Hiemenz, P., 1984. *Polymer Chemistry*. Marcel Dekker Inc., California.
- Hill, T.L., 1986. *An Introduction to Statistical Thermodynamics*. Dover Publications, New York.
- Ivanova, V.P., Heimburg, T., 2001. Histogram method to obtain heat capacities in lipid monolayers, curved bilayers, and membranes containing peptides. *Physical Review E* 63, 1914–1925.
- Janiak, M., Small, D.M., Shipley, G., 1979. Temperature and compositional dependence of structure of hydrated dimyristoyl lecithin. *Journal of Biological Chemistry* 254, 6068–6078.

- Kodama, M., Aoki, H., Miyata, T., 1999. Effect of Na<sup>+</sup> concentration on the subgel phases of negatively charge phosphatidylglycerol. *Biophysical Chemistry* 79, 205–217.
- Kucerka, N., Nieh, M.-P., Katsaras, J., 2011. Fluid phase lipid areas and bilayer thicknesses of commonly used phosphatidylcholines as a function of temperature. *Biochimica et Biophysica Acta* 1808, 2761–2771.
- Kopel, D.J., 1972. Analysis of macromolecular polydispersity in intensity correlation spectroscopy: the method of cumulants. *Chemical Physics* 57, 4814.
- Lamy-Freund, M.T., Riske, K.A., 2003. The peculiar thermo-structural behavior of the anionic lipid DMPG. *Chemistry and Physics of Lipids* 122, 19–32.
- Landau, L.D., Lifshitz, E.M., 2010. *Fluid Mechanics*. Elsevier, China.
- Marsh, D., 1990. *CRC Handbook of Lipid Bilayers*. CRC Press, Florida.
- Pan, J., Heberle, F.A., Tristram-Nagle, S., Szymanski, M., Koepfinger, M., Katsaras, J., Kucerka, N., 2012. Molecular structures of fluid phase phosphatidylglycerol bilayers as determined by small angle neutron and X-ray scattering. *Biochimica et Biophysica Acta* 1818, 2135–2148.
- Riske, K.A., Amaral, L.Q., Lamy, M.T., 2009a. Extensive bilayer perforation coupled with the phase transition region of an anionic phospholipid. *Langmuir* 25 (17), 10083–10091.
- Riske, K.A., Barroso, R.P., Vequi-Suplicy, C.C., Germano, R., Henriques, V.B., Lamy, M.T., 2009b. Lipid bilayer pre-transition as beginning of the melting process. *Biochimica et Biophysica Acta* 1788, 954–963.
- Riske, K.A., Döbereiner, H.G., Lamy, M.T., 2004. Mesoscopic structure in the chain-melting regime of anionic phospholipid vesicles: DMPG. *Biophysical Journal* 86, 3722–3733.
- Riske, K.A., Fernandez, R., Nascimento, O., Bales, B., Lamy-Freund, M.T., 2003. DMPG gel–fluid thermal transition monitored by a phospholipid spin labeled at the acyl chain end. *Chemistry and Physics of Lipids* 124, 69–80.
- Riske, K.A., Nascimento, O., Peric, M., Bales, B., Lamy-Freund, M.T., 1999. Probing DMPG vesicle surface with a cationic aqueous soluble spin label. *Biochimica et Biophysica Acta* 1418, 133–146.
- Riske, K.A., Politi, M., Reed, W., Lamy-Freund, M.T., 1997. Temperature and ionic strength dependent light scattering of DMPG dispersions. *Chemistry and Physics of Lipids* 89, 31–44.
- Rouser, G., Fleischer, S., Yamamoto, A., 1970. Dimensional thin layer chromatographic separation of polar and determination of phospholipids by phosphorus analysis of spot. *Lipids* 5, 494–496.
- Salonen, I.S., Eklund, K.K., Virtanen, J.A., Kinnunen, P.K.J., 1989. Comparison of the effects of NaCl on the thermotropic behaviour of sn-1' and sn-3' stereoisomers of 1,2-dimyristoyl-sn-glycerol-3-phosphatidylglycerol. *Biochimica et Biophysica Acta* 982, 205–215.
- Schneider, M.F., Marsh, D., Janh, W., Kloesgen, B., Heimburg, T., 1999. Network formation of lipid membranes: triggering structural transitions by chain melting. *Proceedings of the National Academy of Sciences of the United States of America* 96, 14312–14317.
- Spinozzi, F., Paccamiccio, L., Mariani, P., Amaral, L.Q., 2010. Melting regime of the anionic phospholipid DMPG: new lamellar phase and porous bilayer model. *Langmuir* 26 (9), 6484–6493.
- Yi, P.N., MacDonald, R.C., 1973. Temperature dependence of optical properties of aqueous dispersions of phosphatidylcholine. *Chemistry and Physics of Lipids* 11, 114–134.
- Zimm, B.H., 1948. The scattering of light and the radial distribution function of high polymer solutions. *Journal of Chemical Physics* 16 (12), 1093–1116.

## Supplementary Material

### Model for a vesicle with ultra-fluid pores

The model we propose for DMPG aggregates along the transition region is a modification of the model suggested by Alakoskela et al. (2010), which consists of perforated spherical vesicles. Holes develop lipid rims, since the bilayer folds inwards to cover hydrocarbon chains, due to the hydrophobic interaction (see Fig. 11). However, we consider lipids in the rims to be in an extremely loose state, in accordance to EPR studies (Riske et al., 2003). This hypothesis allows considering a rim width,  $d'$ , smaller than half the bilayer width  $d$  ( $d' < d$ ) as illustrated in Fig. S1: a thinner rim means fewer lipids in the rim, and more fluid hydrocarbon chains.

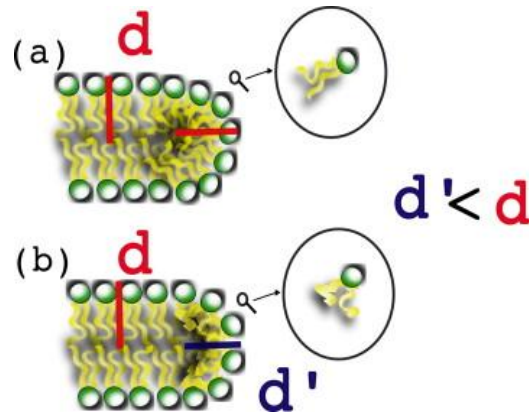


**Fig. S1.** Illustration of a bilayer with a pore. Bilayer and pore rim with similar fluidity ( $d' = d$ ) (a), and pore rim more fluid than bilayer ( $d' < d$ ) (b).

We follow closely the calculations of Alakoskela et al. (2010), under our new hypothesis of lipid rims of increased fluidity. Under the deformation of the integral shell towards a holey spherical shell, lipid volume must be conserved. Thus pore volumes must be subtracted. Conservation of lipid volume, for the holey vesicle, using parameters defined in Fig 11, implies writing

$$V_0(R_{eff}^0) = V_{sph\ shell}(R_{eff}) - n \cdot V_{hole}(r_h) + n \cdot V_{rim}(r_h, d'), \quad (S1)$$

where  $V_0$  is the bilayer volume of the vesicle of radius  $R_{eff}^0$  without perforations, in the gel or fluid phases of the lipid,  $V_{sph\ shell}$  is the volume of the enlarged vesicle shell, in the transition region, disregarding holes,  $n$  is the number of holes of volume  $V_{hole}$  and  $V_{rim}$  is the volume of the hole rim. We write expressions for the three volumes involved.

*Volume of the vesicle shell without holes:* Consider a hollow sphere of external radius  $(R + d)$  and thickness

2d (see Fig 11). The volume of the spherical shell is given by

$$V_{sph\ shell} = (4\pi/3) \cdot \{(R + d) - (R - d)\} = (8\pi d/3) \cdot (3R^2 + d) \quad (S2)$$

*Volume of the pore:* We adopt holes whose radii are defined in terms of an angle  $\theta$  (see Fig. 11). Thus we define a measure for the hole in terms of a radius  $r_h = R \sin\theta$ . The bilayer perforation constitutes a section of a cone and may be calculated as

$$\begin{aligned} V_{hole} &= \int_0^{2\pi} d\varphi \int_0^\pi d\theta \int_{R-d}^{R+d} dr r^2 \sin\theta = 2\pi \cdot [(1 - \cos\theta)/3] \cdot \{(R+d)^3 - (R-d)^3\} = \\ &= (4\pi d/3) \cdot (3R^2 + d^2) \cdot (1 - \cos\theta). \end{aligned} \quad (S3)$$

*Volume of the pore lipid rim:* Finally, we must calculate the volume of the semi-toroidal lipid rim. We consider the cross-section of the toroid centered at point  $P = (R, \theta, \varphi)$ , as in Fig. S2a. The volume of the section of toroid that constitutes the lipid rim is calculated in terms of a new set of variables  $(s, \alpha, \varphi)$  defined with origin at  $P$ , as in Fig. S2b. As can be seen from the figure, we have:

$$\rho = R \sin\theta - s \cos\alpha \quad \text{and} \quad h = s \sin\alpha,$$

so that we may write for  $(x, y, z)$  in terms of the new variables  $(s, \alpha, \varphi)$  the following relations

$$\begin{aligned} x &= \rho \cos\varphi = (R \sin\alpha - s \cos\alpha) \cos\varphi \\ y &= \rho \sin\varphi = (R \sin\alpha - s \cos\alpha) \sin\varphi \\ z &= R \cos\theta - h = R \cos\theta - s \sin\alpha. \end{aligned} \quad (S4)$$

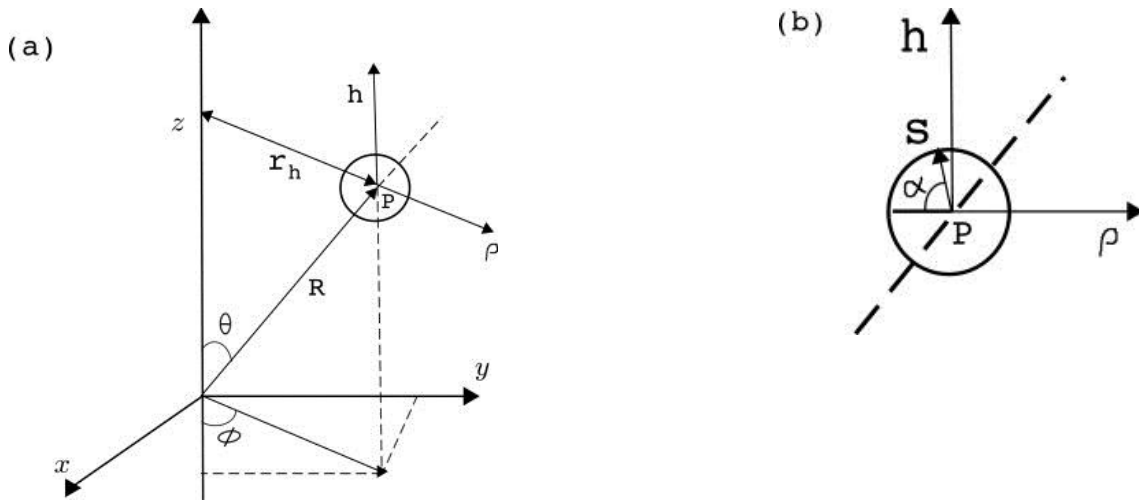


**Fig. S2.** Cross-section of the toroid centered at point  $P = (R, \theta, \varphi)$  (a), and the new set of variables  $(s, \alpha, \varphi)$  defined with the origin at  $P$  (b).

Under these transformations, the rim volume element  $dv_{rim}$  may be calculated from

$$dv_{rim} = \begin{pmatrix} \frac{\partial x}{\partial s} & \frac{\partial y}{\partial s} & \frac{\partial z}{\partial s} \\ \frac{\partial x}{\partial \alpha} & \frac{\partial y}{\partial \alpha} & \frac{\partial z}{\partial \alpha} \\ \frac{\partial x}{\partial \varphi} & \frac{\partial y}{\partial \varphi} & \frac{\partial z}{\partial \varphi} \end{pmatrix} ds d\alpha d\varphi \quad (S5)$$

Calculation of the determinant, Eq. S5, from Eq. S4 yields

$$dv_{rim} = s (R \sin\alpha - s \cos\alpha) ds d\alpha d\varphi. \quad (S6)$$

Thus the lipid rim volume is

$$\begin{aligned} V_{rim} &= \int dv_{rim} = \int_0^{2\pi} d\varphi \int_{-\pi/2+\theta}^{\pi/2+\theta} d\alpha \int_0^{d'} ds s(R \sin\alpha - s \cos\alpha) = \\ &= \pi^2 d'^2 R \sin\theta - 4\pi d'^2 \cos\theta. \end{aligned} \quad (S7)$$

#### *Lipid volume conservation and radius of perforated vesicle*

The different volumes that compose the perforated vesicle may now be added in the equation for conservation of lipid volume, Eq. S1, yielding

$$V_0(R_{eff}^0) = (8\pi d/3).(3R^2+d^2) - n.(4\pi d/3).(3R^2+d^2).(1 - \cos\theta) + n.(\pi^2 d'^2 R \sin\theta - (4\pi d'^3/3).\cos\theta),$$

which we rearrange as

$$4\pi d.[2 - n.(1 - \cos\theta)]R^2 + [n \pi^2 d'^2 \sin\theta]R + \{n.(4\pi/3).(d^3 - d'^3).\cos\theta - n.(4\pi d'^3/3) - V_0(R_{eff}^0)\} = 0 \quad (S8)$$

This quadratic equation may be solved for  $R$ , giving  $R=R(n, d, d', \theta)$ .

The curves for the radius of the perforated vesicle,  $R_{eff} = R + d$ , as a function of the number of holes  $n$  were obtained from the solutions to Eq. S8 for different values of the ratio  $d'/d$ , between rim width  $d'$  and bilayer width  $d$ , and different ratios of pore radius to vesicle radius,  $r_h/R = \sin\theta$ . Integral vesicle radius was taken as  $R_{eff}^0 = 33$  nm and bilayer width was taken as  $d = 1.89$  nm (see text). For  $d' = d$  we reproduce the result of Alakoskela et al.(2010). However, under the assumption of loosely packed rims, based on EPR data (Riske et al., 2003), whose width should be smaller than the bilayer width, much larger effective radii are possible, for the same number of pores, as shown in Fig. 12c.